Electronic Supplementary Material (ESI) for Journal of Materials Chemistry A. This journal is © The Royal Society of Chemistry 2016

Electronic Supplementary Information

For

Hierarchical Forest-like Photoelectrode with ZnO Nanoleaves on Metal Dendrites Array

Li Cheng[a], Qing Chang[b], Yu Chang[a], Nannan Zhang[a], Changyuan Tao[a], Zhaona Wang[b]*

Xing Fan[a]*

[a] College of Chemistry and Chemical Engineering, Chongqing University, Chongqing, 400044, P.R. China

[b] Department of physics, Beijing Normal University, Beijing, 100875, P.R. China

Email: foxcqdx@cqu.edu.cn

Note S1. Experiment Section

1.1 The growth of the nickel dendritic.

The Street-tree-like Ni electrode is grown in a thin layer reactor (Fig. S1a), which is constructed by fixing two electrodes on a glass slide with a tilt angle of 20°. A stainless steel wire (ϕ = 50μm) was used as the cathode, and quaternary alloy ($PbSb_{0.0003}Sn_{0.0003}Ag_{0.0003}$) was used as the anode. The electrolyte flows from cathode to anode slowly and smoothly. The distance between the two electrodes was 1 cm. The thickness of the electrolyte layer was ~30 μm. The electrolyte contained $NiSO_4$ (0.76M), $NiCl_2$ (0.23M), muriatic acids （$10ml\cdot l^{-1}$ w%=37%） and boric acid (0.48M). The initial temperature of the electrolyte is 70°.

The spike-like Ni electrode is grown in an all-round reactor, as shown Fig. S1 b. The quaternary alloy anode was rolled into a cylinder with a diameter of 30mm. The Ni wire (ϕ = 150μm) was employed as the cathode and placed vertically in the center of the quaternary alloy cylinder. The electrolyte was filled up between the cathode and the anode and its height was 20mm. The electrolyte contained $NiSO_4$ (0.76M), $NiCl_2$ (0.23M), muriatic acids （$10ml\cdot l^{-1}$,w%=37%） and boric acid (0.48M). The initial temperature of the electrolyte is 70°.

The micro-forest type Ni electrode is grown in a socket reactor. The internal size of groove is 0.6cm×1cm×3cm. Will serve as the cathode of the Ni plate (0.54cm×4cm) is fixed in the groove, and then put the quaternary alloy anode in front, as shown Fig. S1 c. The distance between the two electrodes was 2 cm. The electrolyte was filled up between the cathode and the anode and its height was 1cm. The electrolyte contained $NiSO_4$ (0.76M), $NiCl_2$ (0.23M), muriatic acids （$10ml\cdot l^{-1}$ w%=37%） and boric acid (0.48M). The initial temperature of the electrolyte is 70°.

1.2 The growth of ZnO nanoleaves on the nickel dendrites.

After cleaned up via distilled water, anhydrous ethanol, in turn, vacuum drying under 80℃ for 1 h, a layer of ZnO nano-seeds was deposited on the nickel dendritic by the spraying

method. After each spray, the dendrite must be placed on the heating plate（210℃）and blow-dried by a blower immediately, in the spraying method. Repeated the two steps of spraying and desiccation, the process is over until the solution（100ml, 0.05M, the mole ratio of Hexamethylene Tetramine and Zinc acetate is 1:1）run out. Then, ZnO-nanorod arrays were grown on the nickel dendritic in the solution (0.03M, the mole ratio of Hexamethylene Tetramine and Zinc acetate is 1:1) at 95°C for 10h in the PTFE lined with stainless steel high pressure reaction kettle.

S2. Calculation of the apparent area of three kinds of dendrite.

The apparent area of a Street-tree-like Ni electrode (*A1*), a spike-like Ni electrode (*A2*) and that of a Micro-forest type Ni electrode (*A3*) could be calculated as follows, respectively.(Fig. S2)

$$A1 = L \times W \quad (1)\ ;$$

$$A2 = L \times D \quad (2)\ ;$$

$$A3 = L \times W \quad (3)\ .$$

Note S3. Fractal growth mechanism.

To examine the fractal feature in the electrodeposition process, the structure of the Ni deposit on the wire electrode or plate electrode, and the corresponding changes with growth voltage during the electrolysis were investigate. The Ni first covers the surface of metal electrode and forms a thin layer of Ni. After then, it continues to grow on the surface of the Ni layer. At first, Miniature balls forms on the surface of the electrode at the onset of electrolysis, and numerous bubbles are produced. When the diameter of the miniature ball exceeds about 35 μm, dendritic branches quickly appear along the surface of the electrode. Subsequently, the dendritic branches grew rapidly, and new subbranches began to appear, which form a typical fractal structure. A dendritic crystal develops on the electrode, with the shape of a forest.

The DLA model has been extensively applied to researches on fractal growth of metals. Based on the DLA model, the fractal feature of deposits depends on the migration of metal ions in the solution [s1-s4]. Particles are generated randomly at any position far from the origin. These particles gradually move toward the origin until they meet the electrode or other metallic particles, thus becoming a part of the cluster. New particles are generated continuously, and this process is repeated to obtain large clusters. For simplification, the walking of one particle could be divided into numerous small steps, with each small step represented by a small vector r_{step}. In the traditional DLA model, r_{step} includes only a random vector, namely,

$$r_{step} = r_{random} \tag{4}$$

If we assume that *rand* is a random number, with 0< *rand* <1, and α is the average step length of the random walking. r_{random} could be expressed as follows, and random walking will be enhanced when α increases. The random walking in the traditional DLA model could be expressed by:

$$r_{random} = \alpha \times [cos(2\pi \times rand) + i \times sin(2\pi \times rand)] \tag{5}$$

A new fixed-length vector component pointing toward the center of the point electrode, r_{radial} is introduced in an attempt to describe the electrodriven centripetal migration.

$$r_{step} = r_{random} + r_{radial} \quad (6)$$

$$r_{radial} = R[cos(\pi + \theta) + i \times sin(\pi + \theta)] \quad (7)$$

R represents the length of the vector component. As *R* increases, the speed of the electrodriven centripetal migration also increases. When R is larger, particles more easily aggregate along the miniature balls of electrode surface because of the electric field. If β is constant, when $R>1$, fractal dimension decrease or even result in forest aggregation. When *R* is low, the electrodeposition speed is slow. Thus, particle migration is mainly determined by the random walking. Particles are easily adsorbed and aggregate on prominent objects, and dendrites are slender and show a low degree of branching. The fractal dimension is also low.

Reference

1 R. F. Voss, M. Tomkiewicz, *J. Electrochem. Soc.* **1985**, 132, 371–375.

2 E. Ben-Jacob, P. Garik, *Nature* **1990**, 343, 523–530.

3 C. A. Marozzi, A. C. Chialvo, *Electrochim. Acta* **2000**, 45, 2111–2120.

4 M. Saitou, W. Oshikawa, A. Makabe, *J. Phys. Chem. Solids* **2002**, 63, 1685–1689.

Note S4. Measurement of the surface area of the dendrite.

Linear voltammetry was employed to measure the actual specific area, during which the current was regarded as being in direct proportion to the surface area of the electrode when the current density was sufficiently small. Linear voltammetry was carried out with Pt as anode and *X*（*X*=Ni-dendritic, Ni-silk）as cathode, and saturated potassium sulfate solution（pH=3）as electrolyte on the electrochemical working station (CHI660D, Shanghai Chenhua), Scan Rate=0.1V/s, and Scan Region is 0-1V.

$$k = \frac{\partial i}{\partial U} \approx \frac{\Delta i}{\Delta U} ; \quad (8)$$

$$\frac{1}{k} = R_1 + R_2 + R_3 ; \quad (9)$$

$$\because R_1 + R_3 \ll R_2,$$

$$\therefore \frac{1}{k} \approx R_2 \text{ and } R_2 = \rho \frac{L}{S_0}$$

$$\therefore S_0 = {}^{\rho L}/_{R_2} = \rho L k ; \quad (10)$$

And $\because k \propto s_0$ and $s_0 \propto s_{cathode}$ （S_{anode}：fixed value）

$$\therefore k \propto s_{cathode}$$

When *X* = Ni-silk, we can get the $k_{Ni\text{-}silk}$ and $S_{Ni\text{-}silk}$;

When *X* = Ni- dendritic, we can get the $k_{Ni\text{-}dendritic}$,

Then $S_{Ni-dendritic} = S_{Ni-silk} \cdot \frac{k_{Ni-dendritic}}{k_{Ni-silk}}$ (11)

Where, *k*: the slope of linear volt-ampere curve in the weak polarization region（Ω^{-1}）; R_1: the resistance of the dendritic（Ω）; R_2: the resistance of the electrolyte（Ω）; R_3: the resistance of Pt（Ω）; *L*： electrode gap（cm）; S_0: the effective cross-sectional area of the electrolyte（cm^2）; ρ: the resistivity of the electrolyte（$\Omega mm^2 \cdot m^{-1}$）; $S_{cathode}$,

S_X：the actual area of cathode (X = Ni-dendritic, Ni-silk; cm^2); S_{anode}: the actual area of anode (Pt; cm^2)

Note S5. The calculation of fractal dimension of Ni dendrites.

The Fractal dimension is widely employed to describe the degree of fractal of an irregular shape. It is calculated as follows.

$$D = -\lim_{a \to 0} \frac{\log N(a)}{\log (a)} \quad (12)$$

Where D is the fractal dimension, N(a) is the number of grids covered by the shape, a is the edge length of the grid (Fig. S6).

For a 1 dimension straight line, the fractal dimension is 1. For a 2 dimension square, the fractal dimension is 2. For a fractal shape above, it is a non-integer in-between 1 and 2. When it is smaller than 1.5, it could be simplified as that the degree of fractal will increase with the D. In this paper, the fractal dimension was calculated by using Image-Pro Plus 6.0 processing software.

Supporting Figures

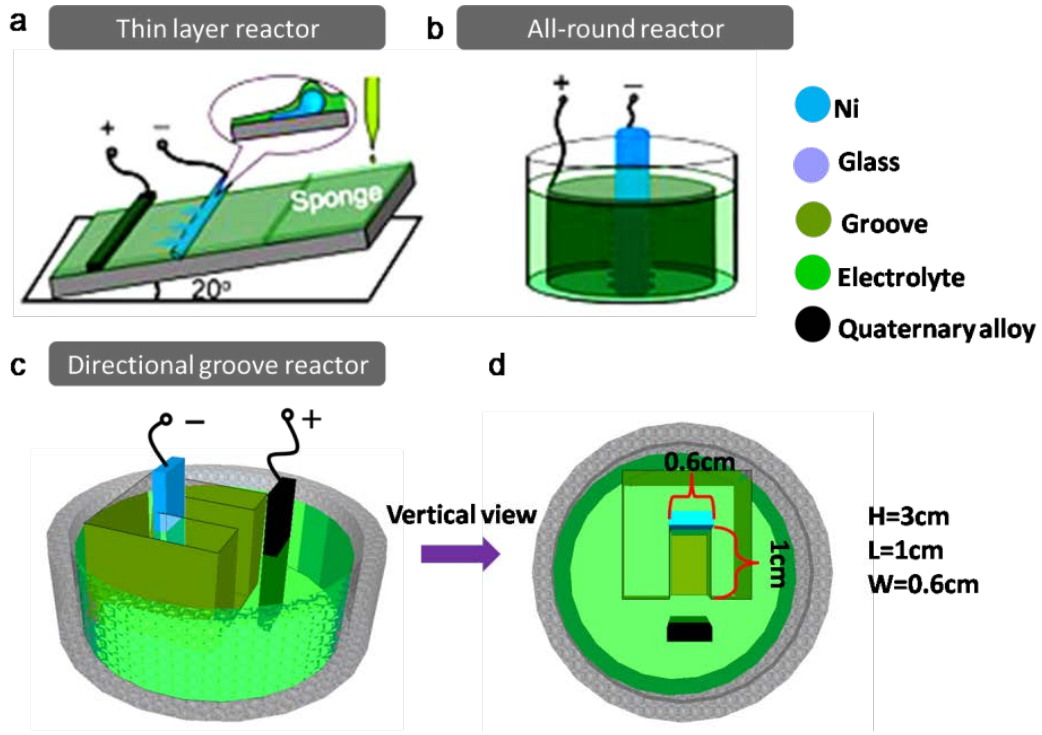

Fig. S1. Schema for the thin layer reactor, the all-round reactor and the socket reactor, respectively. a) Thin layer reator; b) All-round reactor; c) Directional groove reactor; d) The top view of the directional groove reactor.

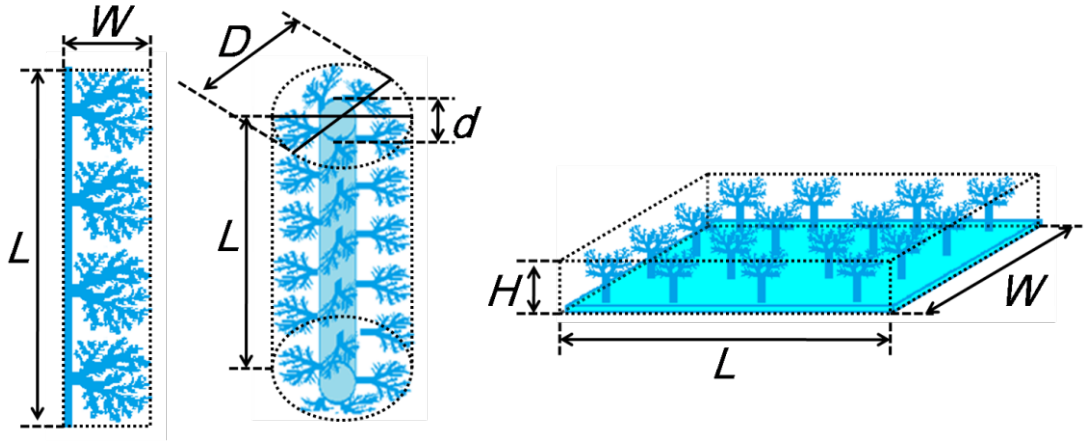

Fig. S2. The apparent area for the type I electrode, the type II electrode and the type III electrode.

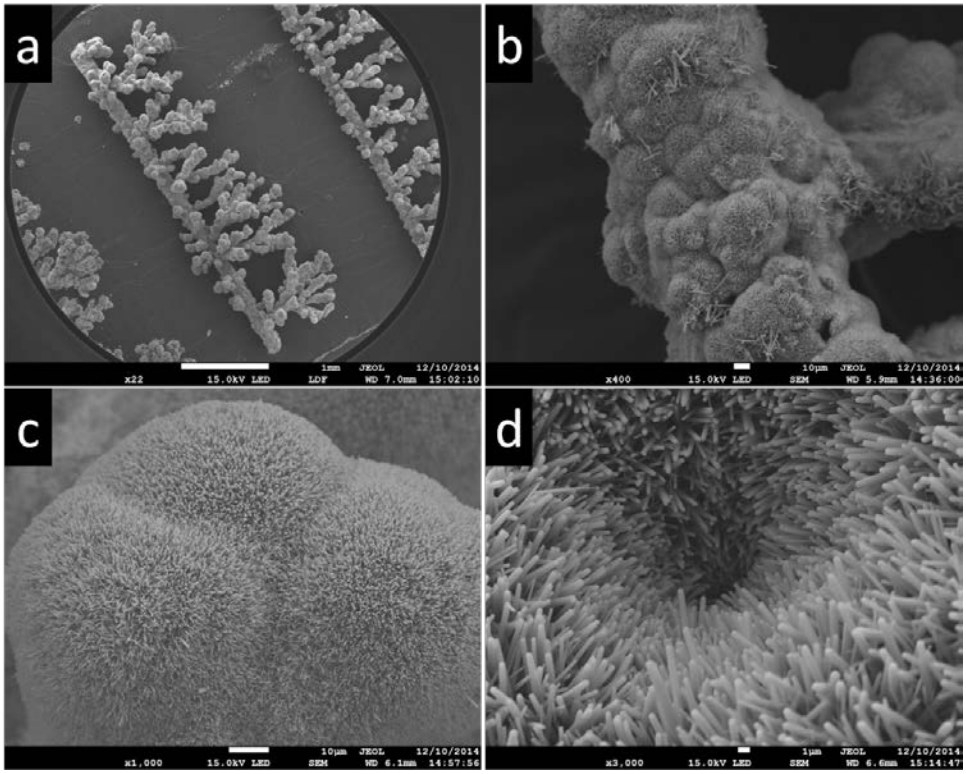

Fig. S3. SEM image of ZnO nano array grown on the street-tree-liake branches.

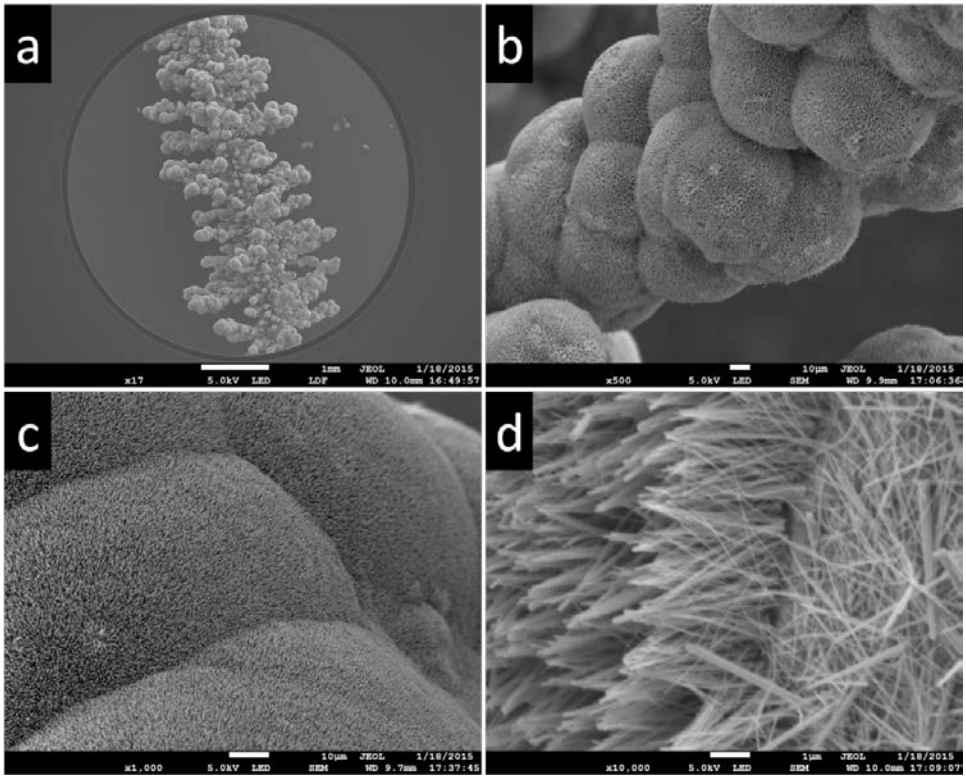

Fig. S4. SEM image of ZnO nano array grown on the spike-like branches.

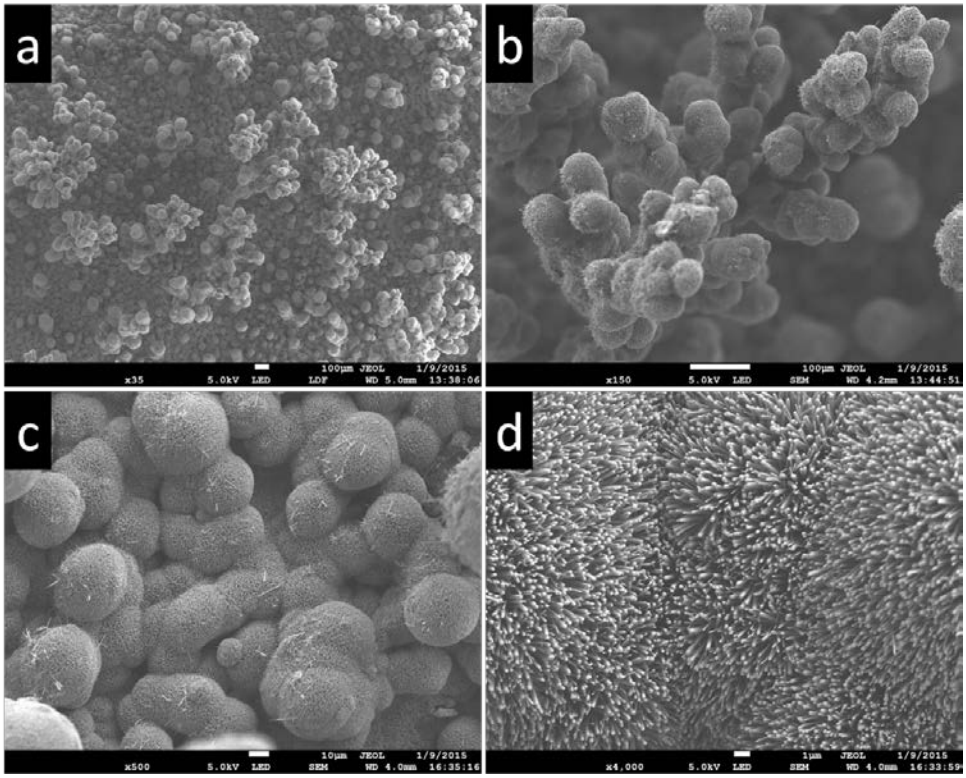

Fig. S5. SEM image of ZnO nano array grown on the micro-forest type branches.

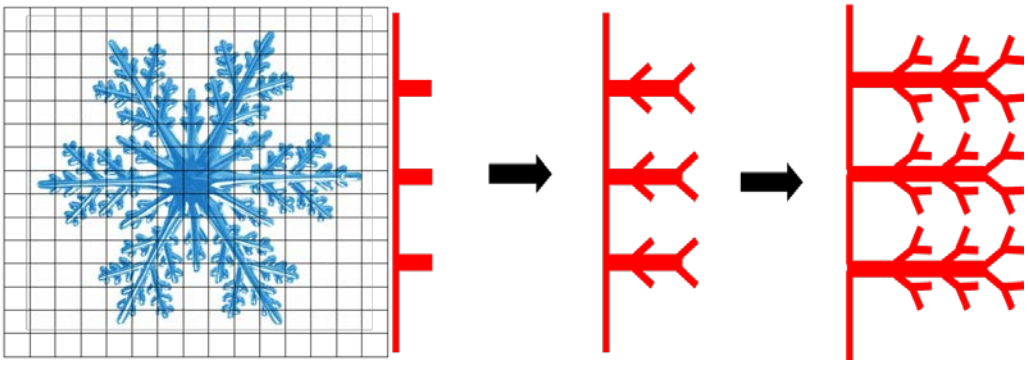

Fig. S6. Left) Illumination of the calculation of fractal dimension; Right) The fractal growth of the dendrites with time.

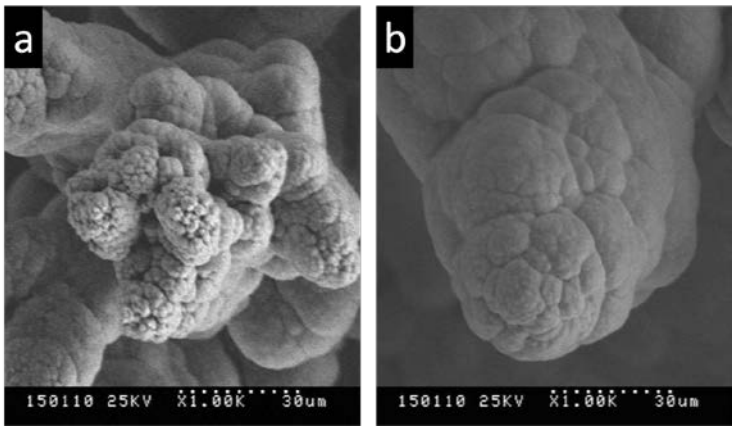

Fig. S7. SEM images of typical Ni branches: a) occurred more at lower pH; b) occurred more at higher pH.

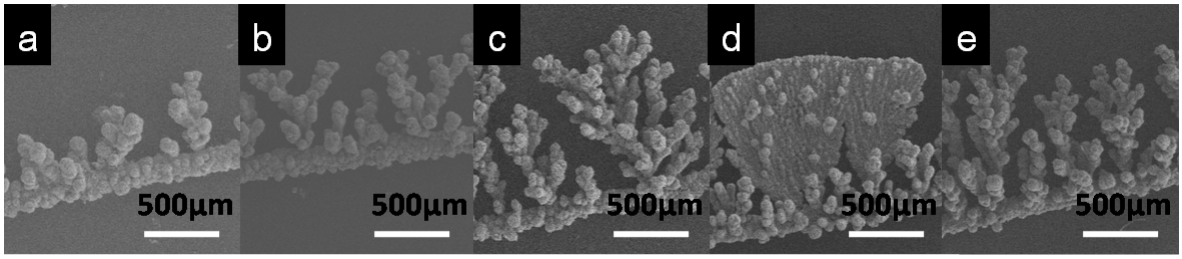

Fig. S8. SEM image of the type I dendrites grown under different growth voltage, a-e): 25V, 30V, 35V, 40V, 45V. Growth voltage is the electrolysis voltage of the electrodeposition reaction.

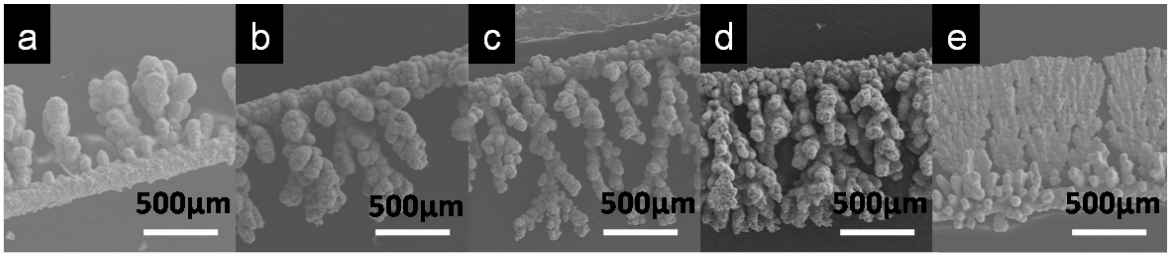

Fig. S9. SEM image of the type I dendrites grown under different initial concentration, a-e): 0.38M, 0.57M, 0.76M, 0.95M, 1.14M. Initial concentration is the concentration of nickel sulfate($NiSO_4$) in the electrolyte, before the start of the reaction.

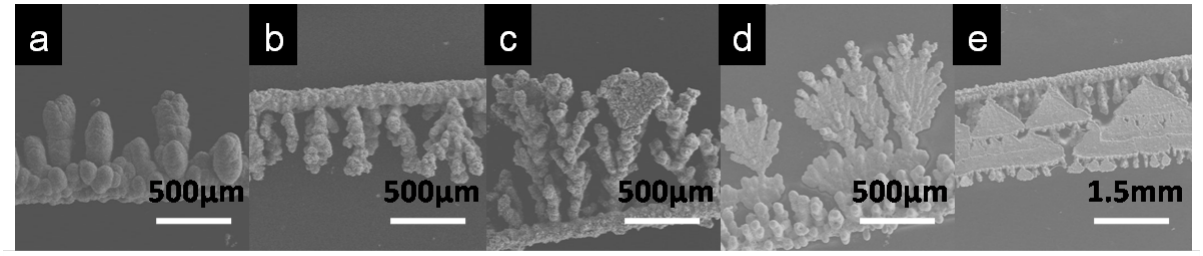

Fig. S10. SEM image of the type I dendrites grown at different growth time, a-e): 20s, 40s, 60s, 80s, 100s. Growth time is the time of the electrodeposition reaction.

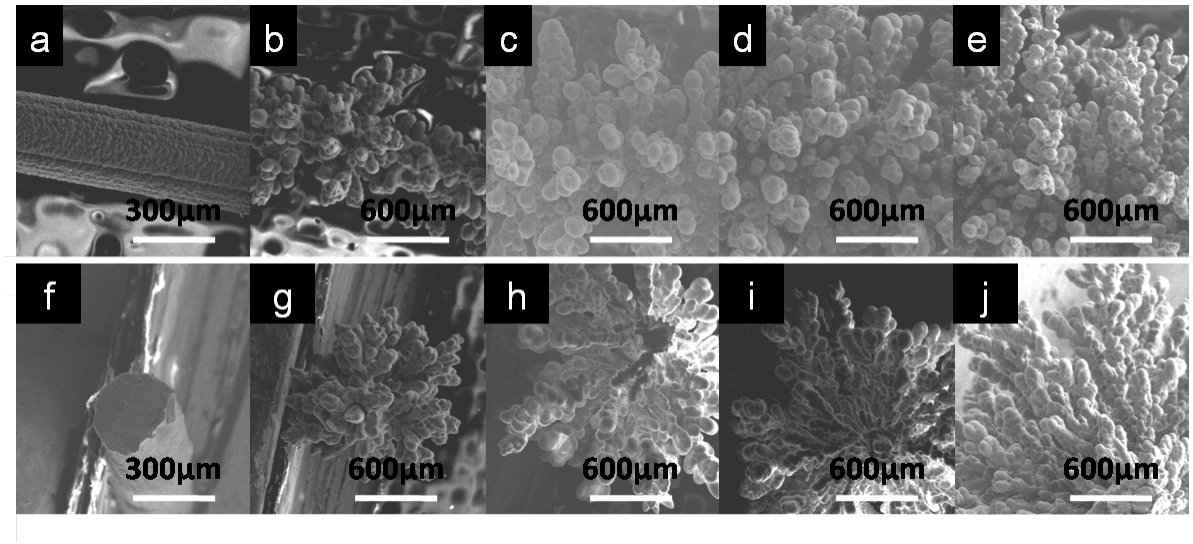

Fig. S11. The type II dendrites grown under different growth voltage, a-e): 25V, 30V, 35V, 40V, 45V, f-j) is the sectional drawing of a-e), respectively. Growth voltage is the electrolysis voltage of the electrodeposition reaction.

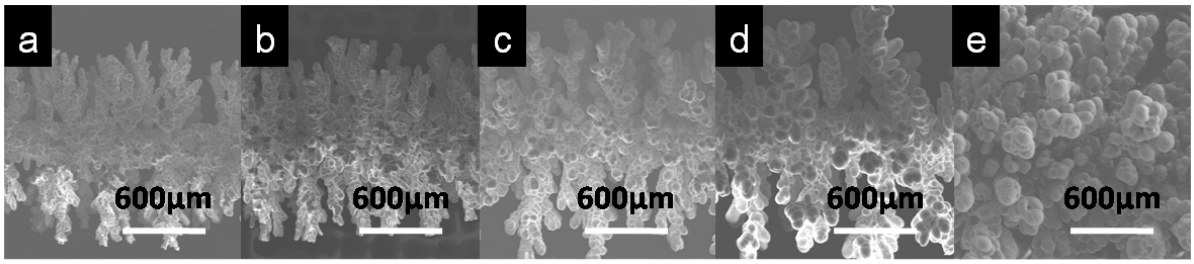

Fig. S12. SEM image of the type II dendrites grown under different ($NiSO_4$) initial concentration, a-e): 0.38M, 0.57M, 0.76M, 0.95M, 1.14M. Initial concentration is the concentration of nickel sulfate($NiSO_4$) in the electrolyte, before the start of the reaction.

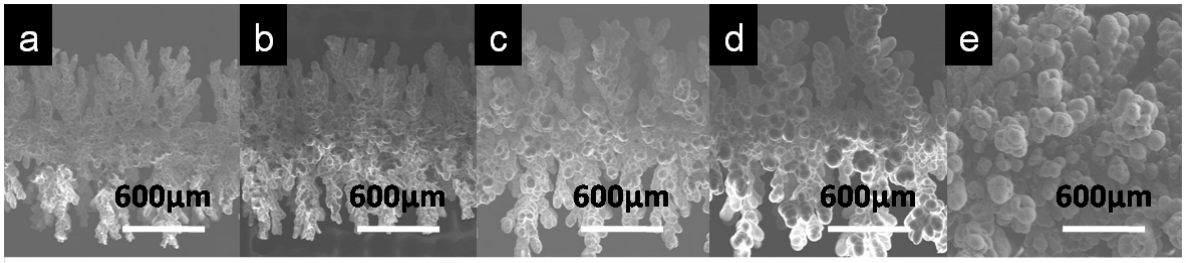

Fig. S13. SEM image of the type II dendrites grown at different growth time, a-e): 90s, 120s, 150s, 180s, 210s. Growth time is the time of the electrodeposition reaction.

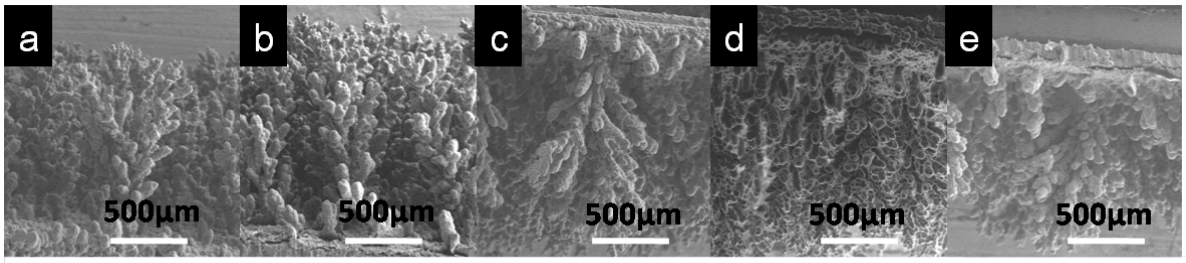

Fig. S14. The type III dendrites grown under different growth voltage, a-e): 50V, 55V, 60V, 65V, 70V. Growth voltage is the electrolysis voltage of the electrodeposition reaction.

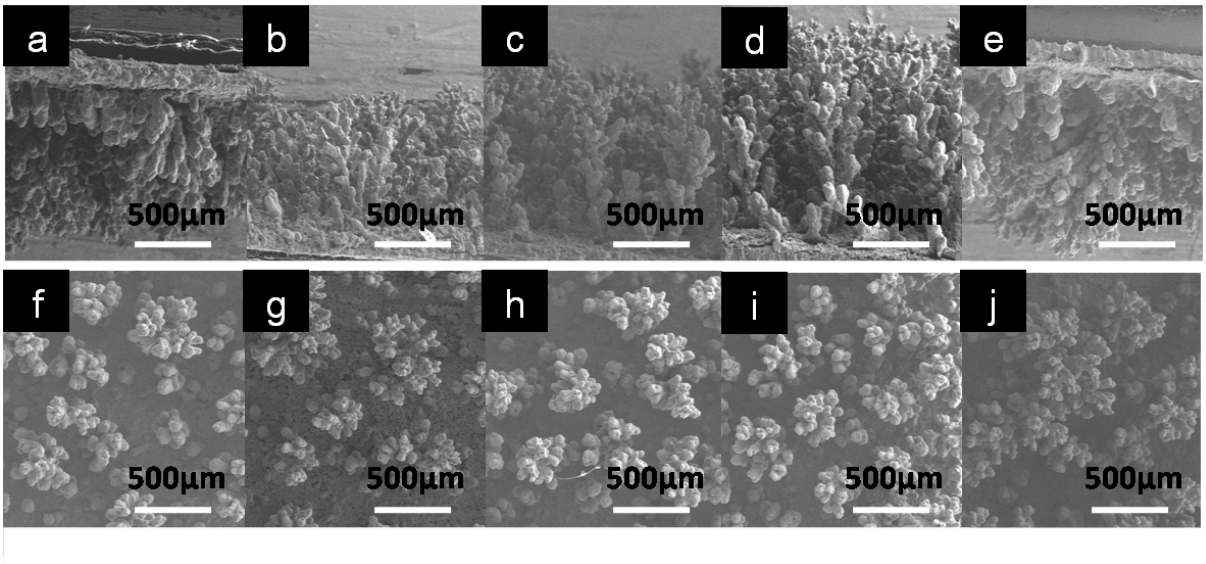

Fig. S15. SEM image of the type III dendrites grown under different ($NiSO_4$) initial concentration, a-e): 0.38M, 0.57M, 0.76M, 0.95M, 1.14M. f-j) is the vertical view of a-e), respectively. Initial concentration is the concentration of nickel sulfate($NiSO_4$) in the electrolyte, before the start of the reaction.

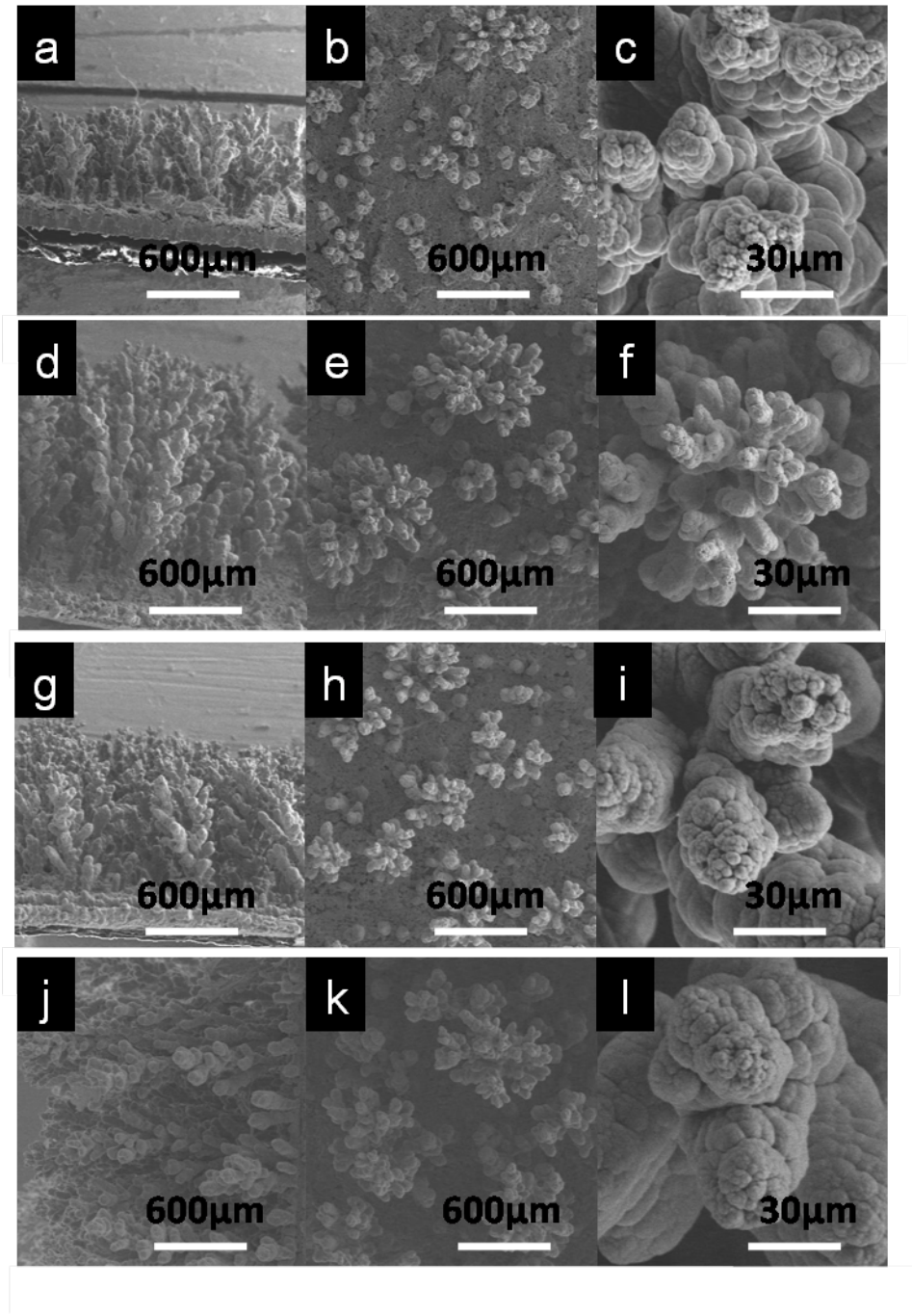

Fig. S16. The type III dendrites grown under different growth time, a-c): 40s; d-f): 60s; g-i): 100s; j-l): 120s. Growth time is the time of the electrodeposition reaction.

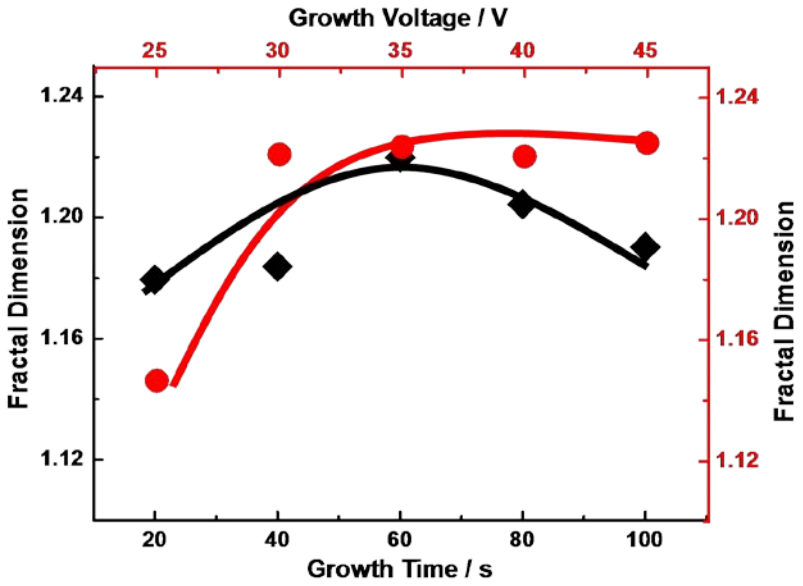

Fig. S17. Influence of growth conditions on fractal dimension of the type I dendrite, red: growth potential; black: growth time.

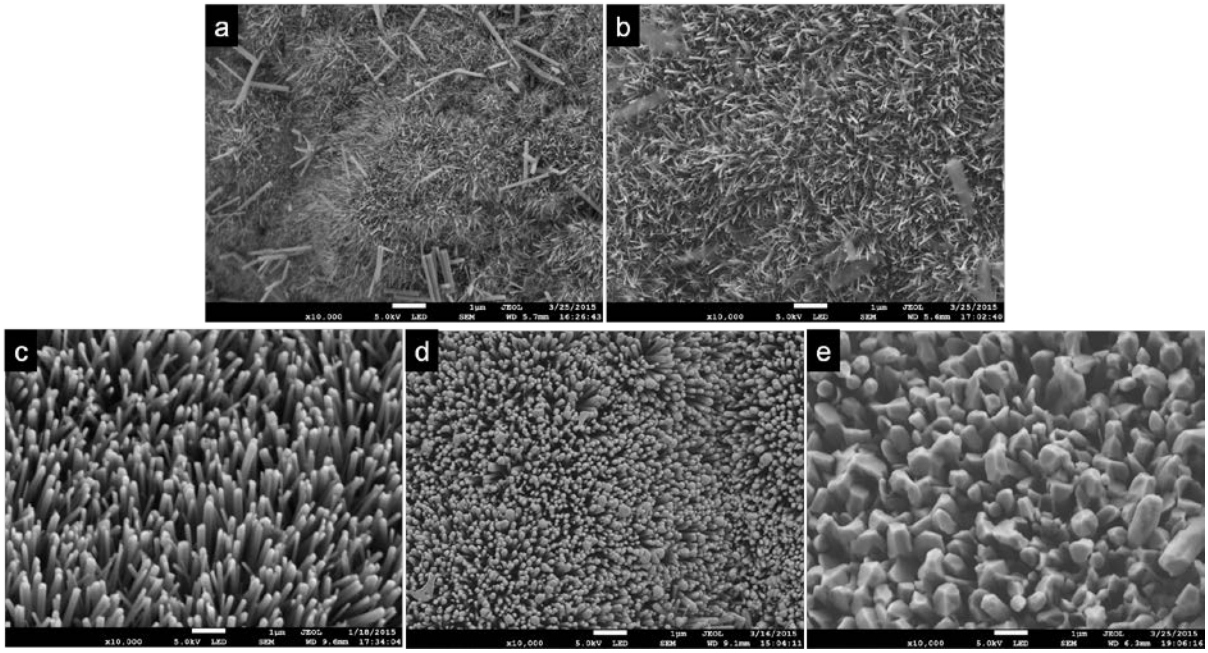

Fig. S18. SEM images of ZnO grown from hydrothermal reaction solutions of different [Zn^{2+}], a-e): 0.01M, 0.02M, 0.03M, 0.04M, 0.05M.

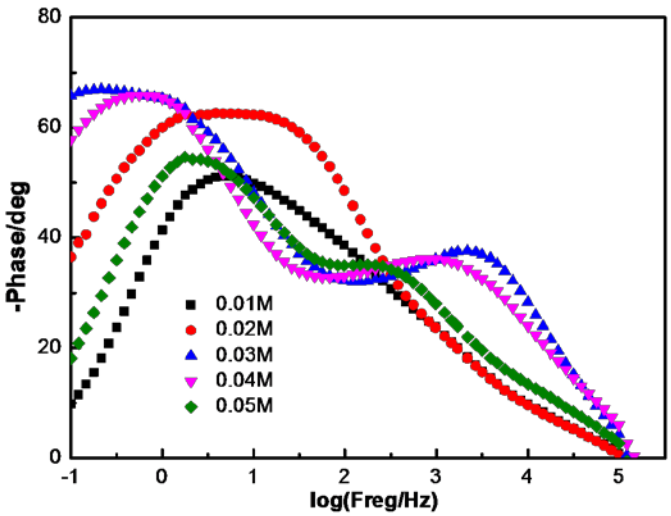

Fig. S19. EIS spectra of the micro-forest type ZnO DSSC photoanodes from hydrothermal reaction solutions of different [Zn^{2+}]. Electrochemical impedance spectroscopy (EIS) was also recorded on the electrochemical working station (CHI660D, Shanghai Chenhua). EIS analysis was conducted at a bias voltage of 0 V in the dark.

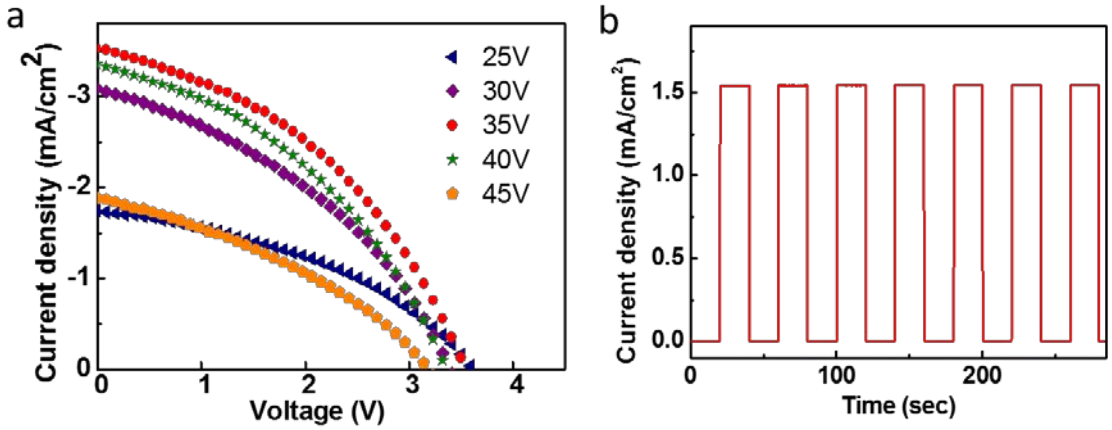

Fig. S20. Left) The current density-voltage of the seri-connected photovoltaic module; Right) Current density–time curve of the integrated water-splitting device without external bias under chopped simulated AM 1.5G 100 mWcm^{-2} illumination

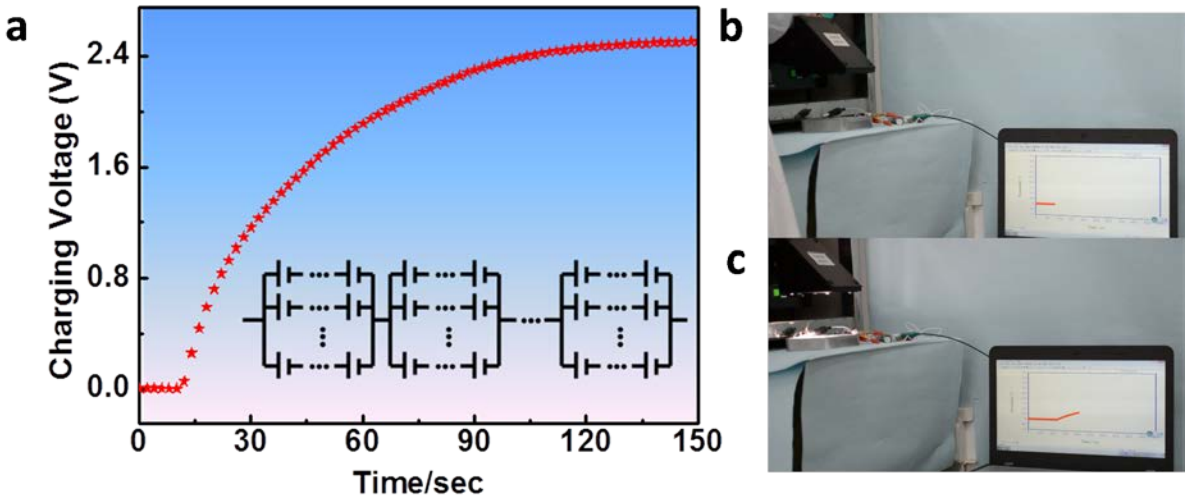

Fig. S21. a) Charging voltage of a 2mF commercial capacitor; b-c) A 2 mF capacitor was charged by the photovoltaic module, b: light off; c: light on.

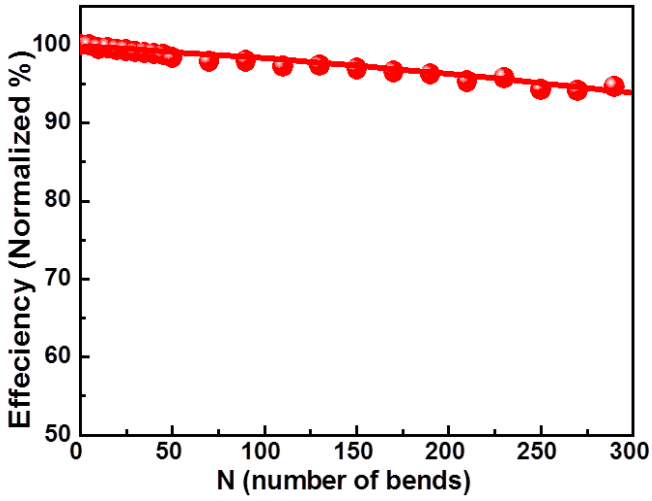

Fig. S22. Influence of bending times on the photovoltaic performance.